Numerical study of the effects of mangrove areas and tidal flats on tides: A case study of Darwin Harbour, Australia

Li Li,[1] Xiao Hua Wang,[1] David Williams,[2] Harvinder Sidhu,[1] and Dehai Song[1]

Received 4 August 2011; revised 21 April 2012; accepted 1 May 2012; published 13 June 2012.

[1] The tidal dynamics of Darwin Harbour, Australia, are simulated using a finite volume coastal ocean model. The calibrated model agreed well with the observed sea surface elevation and current velocity. Results indicate that the harbor's hydrodynamics are driven mainly by the tides, with wind and river inputs playing only small roles. The M_2 tide is dominant, with amplitude 1.7 m and peak current speed 3.0 m s^{-1}. Sensitivity tests using the model indicate that the mangrove areas and tidal flats play crucial roles in modulating tidal amplitudes and phases in the embayments, especially for the shallow water tides such as M_4. Removal of the mangrove areas and tidal flats from Darwin Harbour would dampen the M_2 amplitude due to decreased shoaling effects but generate a 75.0% greater M_4 amplitude in parts of the harbor. Mangrove areas and tidal flats also affect tidal asymmetry through the changing amplitudes and phases of mainly the M_2 and M_4 tides. In Darwin Harbour, tidal asymmetry, measured by elevation and current skewness, would increase by up to 100% if the mangrove areas were removed. If the tidal flats were removed as well, the increase would be 120%. Therefore, reclamation of the mangrove areas and tidal flats may cause sediment siltation as a result of increased flood dominance. Although this study is site-specific, the model and our findings have a wider applicability to the effects of mangrove areas and tidal flats on tides and sediment transport in harbors and estuaries.

Citation: Li, L., X. H. Wang, D. Williams, H. Sidhu, and D. Song (2012), Numerical study of the effects of mangrove areas and tidal flats on tides: A case study of Darwin Harbour, Australia, *J. Geophys. Res.*, *117*, C06011, doi:10.1029/2011JC007494.

1. Introduction

[2] Understanding the hydrodynamics in a harbor is fundamental to the exploration of its transport properties, such as sediment transport, and planning harbor development, such as wharf construction. In particular, the pattern of sediment transport determines the fate of the harbor's morphology, including its mudflats and mangrove zones, the mechanisms of siltation of the navigation channels and the generation of turbid zones. The hydrodynamics in Darwin Harbour are complex because of the complicated shorelines and bathymetry.

[3] Darwin Harbour, a principal exporting harbor, shelters extensive tidal flats and mangrove swamps at its margins. Despite the remarkable ecological and economic importance of this environment, research and field investigations into its hydrodynamics and sediment balance are limited, the exceptions being *Williams* [2009], *Williams et al.* [2006], and *Li et al.* [2011]. The primary aims of our research are to: first build and calibrate a hydrodynamic model of Darwin Harbour against field survey data collected by the Australian Institute of Marine Science (AIMS); and second, use the model to understand the effects of the mangrove areas and tidal flats on the harbor hydrodynamics, including tidal dynamics and tidal asymmetry. The methodology is described in section 2, and the model calibration detailed in section 3. The model results are analyzed in section 4, with conclusions presented in section 5.

2. Methodology

2.1. Model Description

[4] The finite volume coastal ocean model (FVCOM) [*Chen et al.*, 2003] is a three-dimensional hydrodynamic model which uses an unstructured, finite element grid. Compared with structured grid models, such as the Princeton Ocean Model [*Blumberg and Mellor*, 1987] and the Environmental Fluid Dynamics Code [*Hamrick*, 1992], the unstructured grid used by FVCOM is especially suited to Darwin Harbour, which has complex shoreline geometry and dynamic physical processes. As FVCOM solves the three-dimensional momentum, continuity and density equations using a finite volume method, it allows mass conservation to be strictly maintained.

[1]School of Physical, Environmental and Mathematical Sciences, University of New South Wales, Australian Defence Force Academy, Canberra, ACT, Australia.
[2]Australian Institute of Marine Science, Arafura Timor Research Facility, Casuarina, Northern Territory, Australia.

Corresponding author: L. Li, School of Physical, Environmental and Mathematical Sciences, University of New South Wales, Australian Defence Force Academy, Canberra, ACT 2600, Australia. (li.li@student.adfa.edu.au)

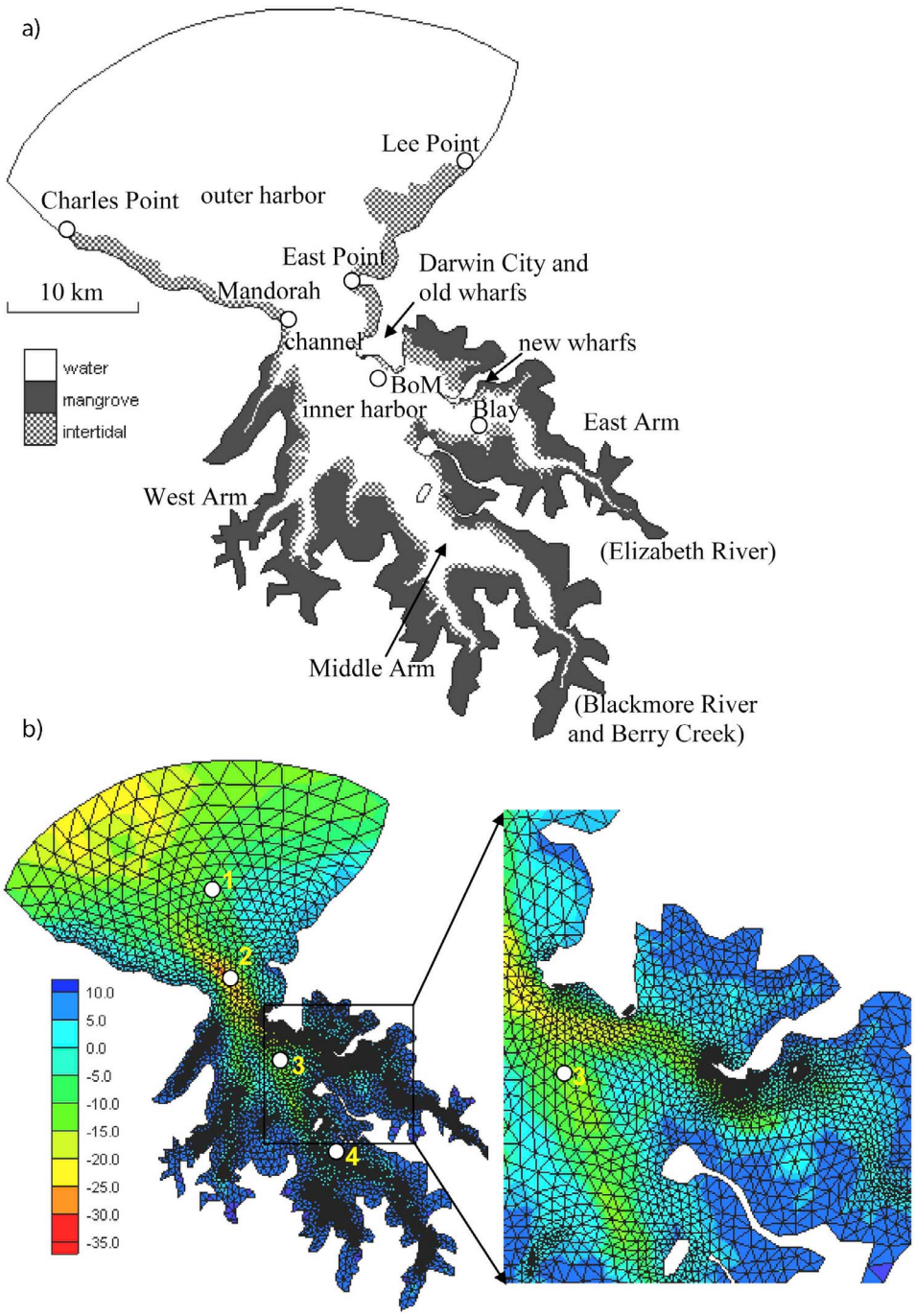

Figure 1. (a) Water areas, intertidal zones, and mangrove areas. (b) Model domain of Darwin Harbour and the grid near the wharfs (inset). Stations 1 to 4 are selected to display vertical current profiles. The depth contours refer to lowest astronomical tides in meters, with positive upward.

[5] A σ-stretched coordinate system is applied in the vertical direction to improve the representation of the complicated bathymetry and obtain a smooth representation of the irregular variable bottom topography. The σ coordinate transformation is defined as $\sigma = \dfrac{z-\zeta}{H+\zeta} = \dfrac{z-\zeta}{D}$, where σ varies from -1 at the bottom to 0 at the surface. The total water column depth is $D = H + \zeta$, where H is the bottom depth and ζ is the height of the free surface, both relative to $z = 0$ (mean sea surface level). The continuity equation is

$$\frac{\partial \zeta}{\partial t} + \frac{\partial (Du)}{\partial x} + \frac{\partial (Dv)}{\partial y} + \frac{\partial w}{\partial \sigma} = 0, \tag{1}$$

where x, y, and σ are the east, north, and vertical coordinates, respectively, and u, v, and w the corresponding velocity components. The model employs the Mellor-Yamada level 2.5

Table 1. Key Model Parameters

Model Parameter	Value
Model time step	1.0 s
Bottom friction coefficient	Minimum 0.0025; 5.0 for mangrove areas
Horizontal diffusion	Smagorinsky scheme
Vertical eddy viscosity	M-Y 2.5 turbulent closure
Nodes, elements, vertical layers	5205, 9666, 20 uniform σ layers
Open boundary condition	Tidal time series from TPXO7.2

turbulence closure scheme [*Mellor and Yamada*, 1982] for vertical mixing and the Smagorinsky scheme for horizontal mixing [*Smagorinsky*, 1963]. The drag coefficient C_d is determined by matching a logarithmic bottom layer to the model at a height z_{ab} above the bottom,

$$C_d = \max\left(\frac{\kappa^2}{(\ln(z_{ab}/z_0))^2},\ 0.0025\right), \quad (2)$$

where $\kappa = 0.4$ is the von Karman constant and z_0 the bottom roughness parameter [*Chen et al.*, 2006].

2.2. Model Configuration

2.2.1. Domain

[6] This study focuses on Darwin Harbour from Charles Point to Lee Point (Figure 1a), with the model domain expanded to include areas outside the mouth of the harbor to keep all open boundary nodes in the open ocean and the mangrove areas in order to check the hydrodynamics there. The water areas, tidal flats, and mangrove areas are shown in Figure 1a. The total area of the mangrove zones is 237.5 km^2 which is 22.4% of the area of the harbor to the high-water mark [*Water Monitoring Branch*, 2005]. Wharf locations are also shown in Figure 1a.

[7] Construction of the unstructured triangular model grid, which consists of 9,666 elements and 5,205 nodes in the horizontal plane, is based on all the available bathymetry and shoreline data from AIMS. Figure 1b shows the model grid for the entire domain; the resolution around the wharfs and in the three arms is especially high. The cell sizes of the domain range from 18 m near the wharfs to 3,300 m at the open boundary. To simulate the vertical profiles of the currents accurately, 20 uniform vertical layers are specified in the water column using the σ coordinate system. Four locations, Stations 1, 2, 3, and 4, in the outer harbor, near the channel, in the inner harbor, and in the Middle Arm, respectively (Figure 1b), are selected to display the tidal current vertical profiles. The observation station Blay is located in the East Arm.

2.2.2. Boundary Conditions and Forcing

[8] The oceanic open boundary is located outside the harbor mouth, extending into the open ocean from Charles Point and Lee Point (Figure 1a). The open boundary conditions for the water level were specified using tidal elevations predicted by the TPXO7.2 global model of ocean tides (available at http://volkov.oce.orst.edu/tides/TPXO7.2.html). Hourly tidal elevations, constructed using four diurnal components (K_1, O_1, P_1, Q_1), four semidiurnal components (M_2, S_2, N_2, K_2), three shallow water components (M_4, MS_4, MN_4) and two long-period components (M_f, M_m), were applied to the open ocean boundary.

[9] The runoff catchment area of the harbor is very small, as that of the main rivers, the Elizabeth and Blackmore Rivers, is only about 120 km^2, 18% of the harbor's total surface area (660 km^2). According to runoff records, if both rivers peaked at the same time, the combined instantaneous runoff would be about 1,000 $m^3\ s^{-1}$. This event would only last for about an hour before falling to a base level of less than 100 $m^3\ s^{-1}$. The probability of this happening is quite low, roughly once in 100 years. In contrast, the peak flow of the spring tide, measured along a line from East Point to Mandorah, is 120,000 $m^3\ s^{-1}$, creating a flood tidal prism that is three orders of magnitude greater than the flood flow's input. Both the Elizabeth and Blackmore Rivers cease to flow during the dry season; Berry Creek does supply fresh water to the Blackmore estuary all year round, but only very little (<1 $m^3\ s^{-1}$).

[10] Therefore, there is no stratification in Darwin Harbour even during the wet season (summer), as the strong tidal velocities cause thorough mixing. Although the upper arms become fresher during flood events, they do not stratify. However, the flood flows do play a role in flushing, and may well affect the resuspension of sediments from the mangrove zone and those that have been moved upstream and deposited during the long dry season (due to the flood dominance of the estuary). The salinity of the water column varies with horizontal position, increasing in the downstream direction until it reaches the background salinity value. This gradual horizontal change in salinity/density can generate density-driven currents, but these are estimated to be less than 0.09 m s^{-1}, about 3.0% of the maximum current observed in the study area.

[11] This paper concentrates on modeling the harbor hydrodynamics in the dry season, when no thermal stratification from the arms to the outer harbor has been observed

Table 2. Descriptions of Experiments

Experiment	Description
1	Reference experiment with all mangrove areas and tidal flats included
2	Without any mangrove areas
3	Without any mangrove areas and tidal flats
4	Without 30% of the total mangrove areas (removal around East Arm)
5	Without 50% of the total mangrove areas (removal around East Arm and the east side of Middle Arm)
6	Without 70% of the total mangrove areas (removal around East Arm and Middle Arm)

Table 3. Observed Current Velocity Skewness γ_c at Station Blay

Vertical Layer	Depth Above Bed (m)	Along-Channel Velocity Skewness
1	1.8	0.16
2	2.8	0.12
3	3.8	0.11
4	4.8	0.11
5	5.8	0.12
6	6.8	0.13
Average layers 1–6		0.12

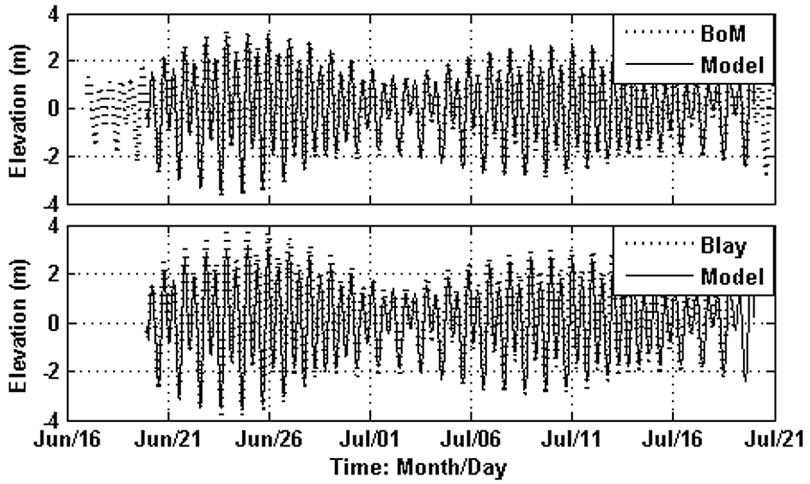

Figure 2. Comparisons of model and observed sea surface elevation near (top) Darwin City (BoM data) and (bottom) Station Blay (AIMS data).

[*Williams*, 2009]. There is a small along-channel salinity gradient created by evapotranspiration; the density currents this generates are again negligible compared with the tidal currents.

[12] Wind has often been considered a predominant driving force for sediment resuspension in many estuaries, especially shallow ones [*Wright et al.*, 1992]. According to *Mehta* [1988], an estuary can be classified into one of three different hydrodynamic regimes based on its tidal range Ω: the dominant hydrodynamic forces are tidal currents, wind waves and wind currents when $\Omega < 1.0$ m; tidal currents and wind waves when $1.0 \leq \Omega \leq 3.0$ m; and tidal currents only when $\Omega > 3.0$ m. Based on this classification, given that the maximum and mean tidal ranges in Darwin Harbour are 7.8 m and 3.7 m, respectively, the hydrodynamics in the harbor are expected to be driven only by tidal currents. Therefore, both wind and heat flux at the free surface boundary are neglected in our model.

[13] The bottom roughness used in the model is calculated according to the water depth. If a node depth is less than 3.0 m, its depth is set to 3.0 m; the bottom drag coefficient C_d is calculated from equation (2). The mangrove zones are treated differently from the water areas and tidal flats due to the larger drag forces caused by mangrove trees and their roots [*Mazda et al.*, 1997]. According to field experience and *Mazda et al.* [1997], C_d ranges from about 1.0 to 10.0 depending on the observation site, mangrove species and tidal conditions. In this study, the median value $C_d = 5.0$ is set for the mangrove areas.

2.2.3. Initial Conditions

[14] The model is initialized with constant values for salinity of 33 psu and for temperature of 25°C, typical of the harbor's mean temperature and salinity during the dry season. Together with the assumptions of no river inflow and zero heat flux at the surface, these values result in barotropic conditions in the model. The model was run for 31 days, from 20 June 2009 to 21 July 2009; its key parameters are summarized in Table 1.

2.2.4. Model Runs and Sensitivity Tests

[15] In order to check the effects of the mangrove areas and tidal flats on tides in the harbor, three numerical experiments using the model were designed: in Experiment 1, the model was run with all mangrove areas and tidal flats included; in Experiments 2 and 3, the mangrove areas and the mangrove areas plus tidal flats, respectively, were removed from the model.

[16] Three further sensitivity experiments were run to examine the effect of mangrove areas in more detail by progressively removing them from the model: in Experiment 4, about 30% of the total mangrove area was removed, from around the East Arm; in Experiment 5, about 50%, from around the East Arm and the east side of the Middle Arm; and in Experiment 6, about 70%, from around the East Arm and Middle Arm. Descriptions of all experiments are given in Table 2. These mangrove removal scenarios are in

Table 4. Comparison of Model and Observed Tidal Harmonic Parameters Near Darwin City[a]

	Amplitude (m)			Phase (deg)		
Main Tidal Constituent	Observed	Model	Amplitude Deviation (%)	Observed	Model	Phase Deviation (deg)
O_1	0.33	0.30	−9.1	190.1	187.2	−2.9
K_1	0.58	0.53	−8.6	200.5	196.2	−4.3
N_2	0.35	0.29	−17.1	228.4	212.4	−16.0
M_2	1.85	1.70	−8.1	249.3	242.1	−7.2
S_2	0.96	0.93	−3.1	298.1	299.6	1.5
K_2	0.27	0.25	−7.4	296.0	322.0	26.0
M_4	0.05	0.04	−20.0	107.1	46.4	−60.7

[a]Data from the Bureau of Meteorology.

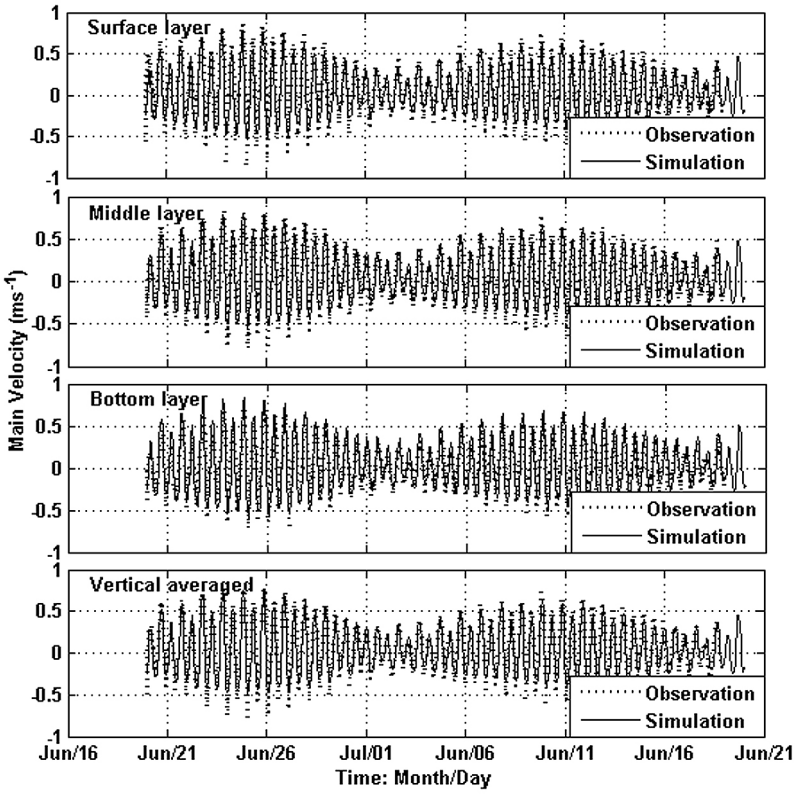

Figure 3. Comparisons of model and observed (AIMS) along-channel velocities in East Arm near Station Blay.

accordance with those which may occur due to development of the local economy, because almost all the social and economic activities of Darwin take place near the East Arm.

2.3. Tidal Asymmetry

[17] According to *Walton* [2002], if the duration of the falling tide is shorter/longer than that of the corresponding rising tide, thereby leading to a stronger ebb/flood current, the system is referred to as ebb/flood dominant, respectively. The tidal duration asymmetry γ_1 can be calculated using the normalized sample skewness of the tidal elevation time derivative $\left(\frac{\partial \zeta}{\partial t} = \zeta'\right)$ [*Nidzieko*, 2010]:

$$\gamma_1 \equiv \frac{\mu_3}{\delta^3} = \frac{\frac{1}{T-1}\sum_{t=1}^{T}\left(\zeta'_t - \overline{\zeta'}\right)^3}{\left[\frac{1}{T-1}\sum_{t=1}^{T}\left(\zeta'_t - \overline{\zeta'}\right)^2\right]^{3/2}}, \tag{3}$$

where ζ is the sea surface elevation (SSE); μ_3 is the third sample moment about the mean; and δ is the standard deviation [*Emery and Thomson*, 2001]. The total time over which the model was run, T, was 31 days in this paper. The

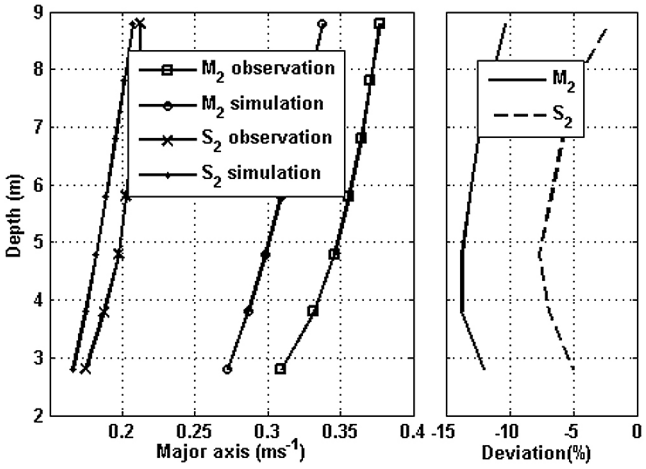

Figure 4. Comparisons of model and observed vertical current profiles of the M_2 and S_2 tides in East Arm near Station Blay.

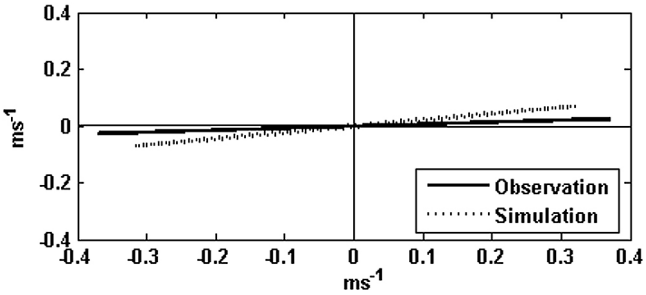

Figure 5. Comparisons of model and observed near-surface current orientations of the M_2 tide in East Arm near Station Blay.

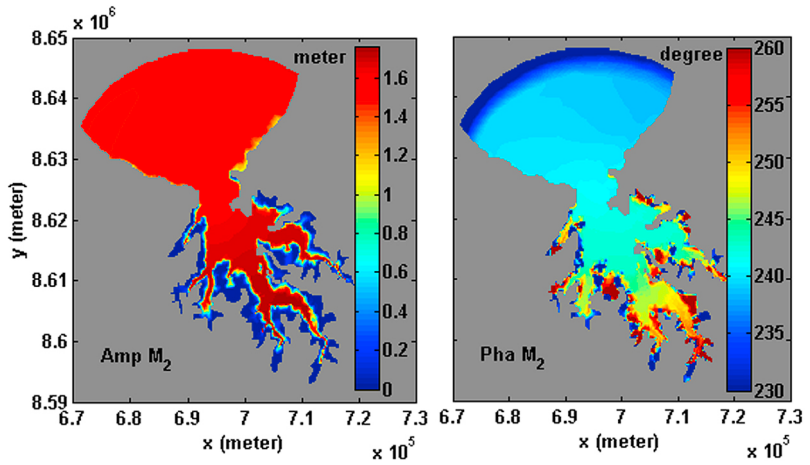

Figure 6. Amplitudes and phases of the M_2 tide from sea surface elevation from the model. The coordinates come from the Mercator projection.

ebb tide duration is shorter if $\gamma_1 < 0$, the flood tide duration shorter if $\gamma_1 > 0$.

[18] In an estuarine environment with the tidal elevation and tidal currents generally 90° out of phase, the asymmetry γ_1 computed from tidal elevation will be similar to the asymmetry γ_c calculated from currents in the absence of river flow, stratification and bathymetry effects [*Nidzieko*, 2010], as is the case for Darwin Harbour.

[19] According to *Song et al.* [2011], γ_1 can also be calculated using the amplitudes, frequencies and phases of all the components of the astronomical tides by

$$\gamma_1 = \frac{\sum_{\omega_i+\omega_j=\omega_k} \frac{3}{2} a_i\omega_i a_j\omega_j a_k\omega_k \sin\left(\varphi_i+\varphi_j-\varphi_k\right) + \sum_{2\omega_i=\omega_j} \frac{3}{4} a_i^2\omega_i^2 a_j\omega_j \sin\left(2\varphi_i-\varphi_j\right)}{\left(\frac{1}{2}\sum_{i=1}^{N} a_i^2\omega_i^2\right)^{3/2}}, \quad (4)$$

where a_i, ω_i, and φ_i are the tidal amplitudes, frequencies, and phases of the respective components of the astronomical tides. In this study, the M_2/M_4 combination makes the most significant contribution. Other constituent combinations only play minor roles and can be neglected. If only these two constituents are considered, the tidal asymmetry γ_1 may be approximated by γ_{M_2/M_4}, where [*Song et al.*, 2011]

$$\gamma_{M_2/M_4} = \frac{\frac{3}{2} a_{M_2}^2 a_{M_4} \sin\left(2\varphi_{M_2}-\varphi_{M_4}\right)}{\left[\frac{1}{2}\left(a_{M_2}^2+4a_{M_4}^2\right)\right]^{3/2}}. \quad (5)$$

The approximation γ_{M_2/M_4} is used here in analyzing the controlling factors of tidal asymmetry in the harbor.

[20] The skewness γ_{M_2/M_4}, calculated from the SSE data near Station Blay is positive (0.06), which indicates flood dominance [*Walton*, 2002]. The skewness γ_c of each of the

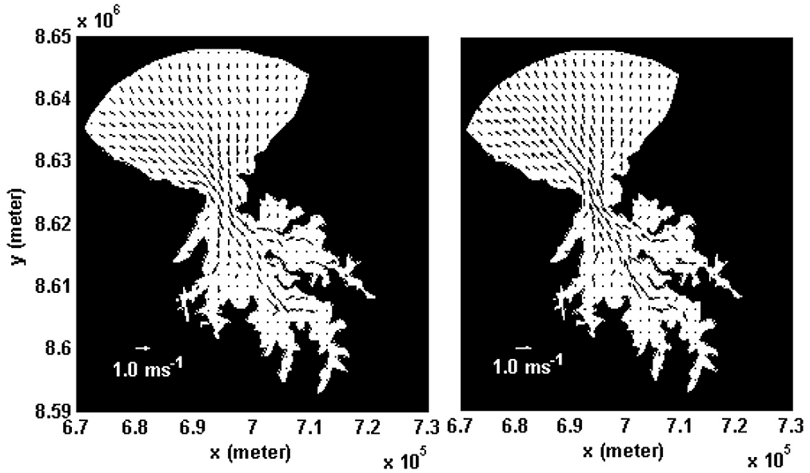

Figure 7. Vertically averaged velocities of the (left) spring flood and (right) ebb currents from the model.

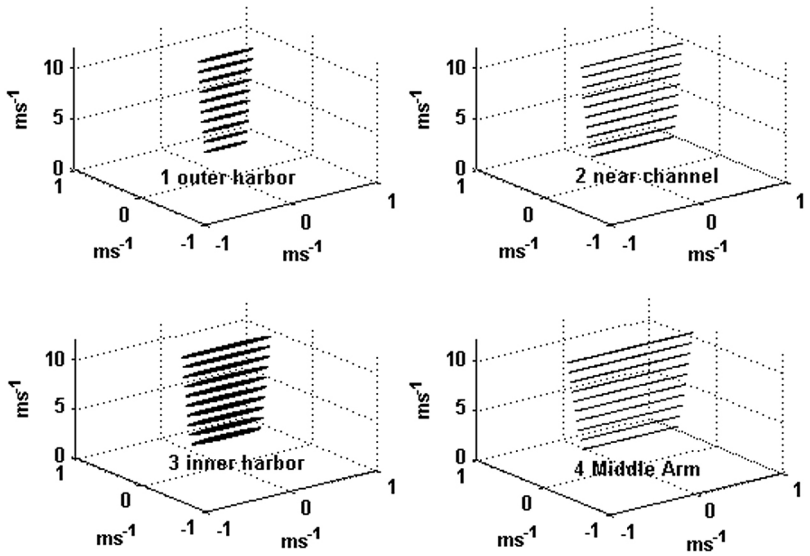

Figure 8. Vertical distribution of the M_2 tidal current ellipses at the four stations shown in Figure 1 from the model.

observed along-channel current velocities at Station Blay is shown in Table 3; these values indicate flood dominance at all depths. In Darwin Harbour, γ_c is larger than γ_{M_2/M_4}, because the bathymetry can produce local asymmetry in tidal currents that is sometimes not manifested in the free surface records [*Godin*, 1991].

3. Model Calibration

3.1. Sea Surface Elevation

[21] The hourly SSE data for the years 1992–2009 from the observation station of the Bureau of Meteorology (BoM, Figure 1a) were analyzed to study the principal tidal characteristics of the harbor. The AIMS data from the Nortek ADCP at Station Blay (Figure 1a) were taken in the period 20 June to 19 July 2009 at 10 min intervals. Tidal data from both the BoM and AIMS were used to calibrate the model results. Figure 2 shows the predicted SSE time series, which agree well with the field data from the BoM (top) and Station Blay (bottom).

[22] Comparisons of the amplitudes and phases for the SSEs of the main tidal constituents, M_2, S_2, K_1, N_2, O_1, and K_2 near Darwin City as observed and from the model, are shown in Table 4. The harmonic constants are averaged from the annual harmonic analyses from 1992 to 2009. Of these tidal constituents, M_2 is the predominant tide, which indicates that the harbor is a semidiurnal environment. Table 4 demonstrates solid agreement between the model and observed amplitudes and phases. The deviations of the model M_2 and S_2 amplitudes/phases from those observed are 8.1%/7.2° and 3.1%/1.5°, respectively. The large discrepancy between the observed and modeled N_2 and K_2 phases may be caused by the fact that the tidal analysis is based on a 1 month time interval, and it is therefore unable accurately to resolve these constituents.

3.2. Current Velocity

[23] Current velocity validations were conducted at the bottom, middle, and surface levels, and are shown in Figure 3. Comparisons of the predicted and observed along-channel velocities in the East Arm near Station Blay indicate that the model predicts the velocity magnitudes and phases very well.

[24] The vertical current profiles of the M_2 and S_2 tides from the model and the observed data are shown in Figure 4, along with the maximum current speeds at Station Blay (Figure 4, left). The model values are in solid agreement with the observed values in both magnitude and trend from the bottom to the surface, with model deviations from the observations being no more than 15% (Figure 4, right). In addition, the predicted orientations of the surface current ellipses of the M_2 tide match well with those from the observed data, as shown in Figure 5. Although only the orientation near the surface is shown here, those at the other depths have similar directions.

[25] In conclusion, the model results show reasonably good agreement with the observed values, with acceptable errors, for SSEs, currents, amplitudes and phases of the M_2 and S_2 tidal constituents. As a result, we believe that the model can be used to simulate accurately the water flow dynamics in the harbor.

4. Model Results and Discussion

4.1. Tides in Darwin Harbour

[26] The surface amplitudes and phases of the M_2 tide are shown in Figure 6. The amplitudes increase gradually from about 1.4 m in the outer harbor to about 1.7 m in the arms, then decrease to about 1.0 m in the tidal flats, finally decreasing to almost zero in the mangrove areas. This large decrease in amplitude is due to the dramatic bottom dissipation in mangrove zones with their high C_d values. The phase increases from the outer harbor to the arms, with the extreme low and high values in the mangrove areas, driven by the wetting-drying process.

[27] Figure 7 shows the vertically averaged velocities of the spring flood and ebb currents from the model. For clarity, the velocity vectors are interpolated to an averaged grid

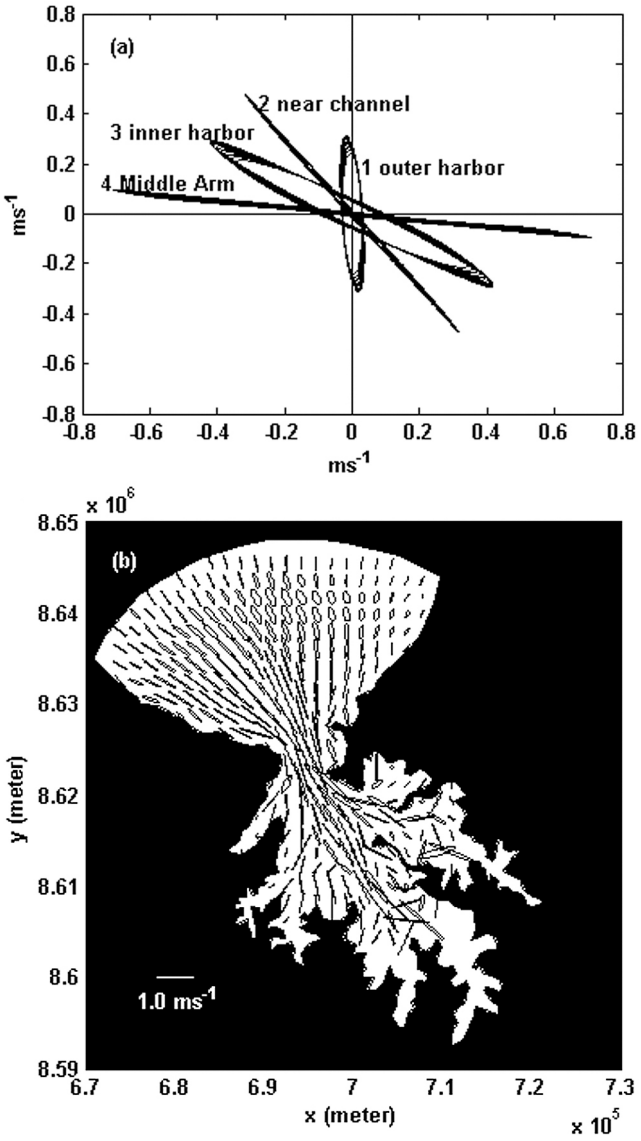

Figure 9. (a) M_2 tidal current ellipse orientations at the four stations from the model. (b) M_2 tidal current ellipse surface distributions from the model.

with horizontal resolution of about 2.0 km. The current velocities reach a maximum in the Middle Arm, with a peak of more than 3.0 m s^{-1}. In the inner harbor and arms, the water flow patterns are in accordance with the shoreline. Current speeds fall to zero in the mangrove regions because of the large amount of bottom friction (high C_d value).

[28] Variations in the M_2 tidal current ellipses at the different vertical layers at the four selected locations are shown in Figure 8. At the surface, the maximum speed of the M_2 tidal current increases from the outer harbor (0.3 m s^{-1}) to the channel (0.6 m s^{-1}), then decreases in the inner harbor (0.5 m s^{-1}); it reaches its maximum in the Middle Arm, roughly 1.3 m s^{-1}. The maximum current speeds of the M_2 tide decrease from the surface to the bottom at all four locations because of friction at the bottom; Middle Arm experiences the most rapid decrease, 33.5%, as it has the shallowest water, while the location near the channel has the smallest decrease, 24.8%, because of its deep water column.

[29] The orientations of the M_2 tidal current ellipses for all the vertical layers at the four locations are shown in Figure 9a. The currents in all the layers are roughly in the same northwest-southeast direction, from the surface to the bottom, except at Station 1. The current ellipse rotates more than 70° in an anticlockwise direction from Station 1 to Station 4. The current ellipse orientations are controlled by the shoreline and navigation channel, which has been deepened in the northwest-southeast direction along the channel to the East Arm. As Station 1 is in the outer harbor mouth, away from the land boundary, the controlling effect of the shoreline is less there than at Stations 2–4. The surface distribution and characteristics of the M_2 tidal current ellipses are shown in Figure 9b. The current ellipses in the outer and inner harbors are elliptical, while those in the channel and the three arms are rectilinear.

4.2. Effects of Mangrove Areas and Tidal Flats on Tides

4.2.1. Variation in the M_2 Tide

[30] If the mangrove areas (Experiment 2; Table 2) and mangrove areas and tidal flats (Experiment 3) are removed, the amplitudes in the outer harbor increase by 0.01 m (0.5%) and 0.02 m (1.0%), respectively (compared with the reference, Experiment 1), due to reduced tidal choking [*Li et al.*, 2011]; those in the inner harbor decrease by 0.01 m (0.5%) and 0.02 m (1.0%), respectively, because of the reduced shoaling effect.

[31] Compared with Experiment 1, the M_2 phase advances (by up to 2° or 4 min) when the mangrove areas are removed (Experiment 2), and advances further (by up to 5° or 10 min) when the tidal flats are also removed (Experiment 3). Again this is due to a reduced tidal choking effect. When the inner harbor capacity is reduced, the tidal choking effect is diminished.

4.2.2. Variation in the M_4 Tide

[32] The M_4 amplitude differences between Experiment 2 and Experiment 1 (Figure 10) increase from the outer to the inner harbor and the arms, with a similar difference between Experiment 3 and Experiment 1 (Figure 11). Compared with Experiment 1, the amplitude of M_4 in the arms increases by 0.02 m (50.0%) when the mangrove areas are removed (Experiment 2), and by 0.03 m (75.0%) when the tidal flats are also removed (Experiment 3).

[33] In the inner harbor, when the mangrove areas (Experiment 2)/mangrove areas and tidal flats (Experiment 3) are removed, the M_4 phase advances by 20° (18 min)/40° (42 min), respectively, compared with Experiment 1. However, in the outer harbor, they are delayed in both Experiments 2 and 3 compared with Experiment 1.

[34] As the M_4 overtide is generated by the self-interactions of the M_2 tide [*Egbert et al.*, 2010], its changes in amplitude and phase result from those in M_2. In both Experiments 2 and 3, its amplitude increases and its phase advances in the inner harbor compared with the values in Experiment 1.

[35] The data from Station Blay in the East Arm were used to examine the variations in the tides in detail (Tables 5 and 6). In Experiment 2, the M_2 amplitude and phase change slightly from those of the reference model (Experiment 1); the M_4 tidal amplitude/phase increases/advances by 50%/16°, respectively. Removing the mangrove areas will cause the M_2/M_4 currents to dramatically decrease, by 22.9%/20.0%,

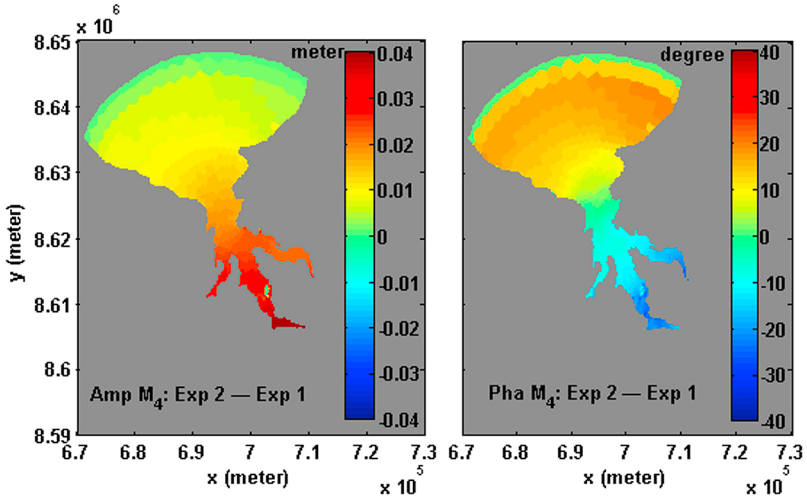

Figure 10. Changes in the M_4 amplitudes and phases when the mangrove areas are removed (Experiment 2 minus Experiment 1).

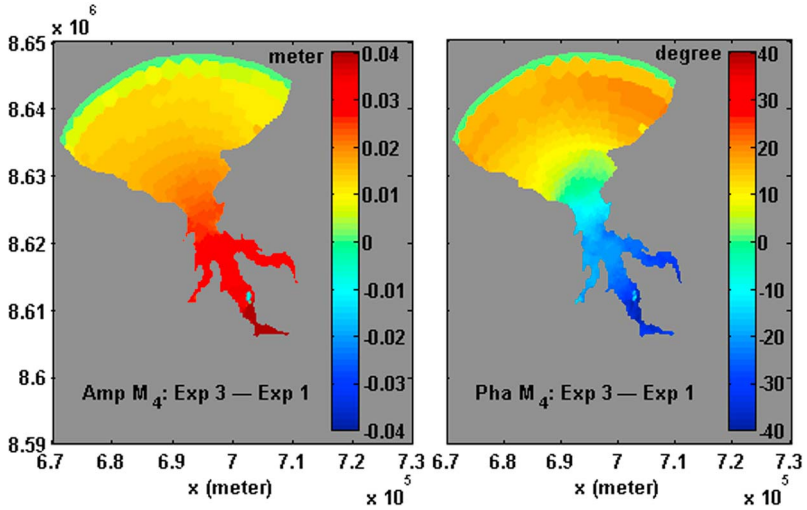

Figure 11. Changes in the M_4 amplitudes and phases when the mangrove areas and tidal flats are removed (Experiment 3 minus Experiment 1).

Table 5. Model and Observed Sea Surface Elevation Amplitudes and Phases of the M_2 and M_4 Tides Near Station Blay

Description of Experiment	M_2 Tide		M_4 Tide	
	Amplitude (m)	Phase[a] (deg)	Amplitude (m)	Phase[a] (deg)
Observed (Station Blay)	1.92	249.4	0.06	113.0
Exp. 1: Reference model	1.74	242.5	0.04	55.1
Exp. 2: Without any mangrove areas	1.73	242.3	0.06	39.4
Exp. 3: Without any mangrove areas and tidal flats	1.71	240.3	0.07	27.5

[a]Phase angles refer to Greenwich mean time (GMT).

Table 6. Model and Observed Vertically Averaged Tidal Current Major Axes of the M_2 and M_4 Constituents Near Station Blay

Description of Experiment	M_2 Tide		M_4 Tide	
	Vmajor[a] (m s^{-1})	Phase[b] (deg)	Vmajor[a] (m s^{-1})	Phase[b] (deg)
Observed (Station Blay)	0.35	167.1	0.06	54.1
Exp. 1: Reference model	0.35	163.6	0.05	342.6
Exp. 2: Without any mangrove areas	0.27	163.0	0.04	312.9
Exp. 3: Without any mangrove areas and tidal flats	0.19	162.7	0.03	287.7

[a]Vmajor = major axis of tidal current.
[b]Phase angles refer to Greenwich mean time (GMT).

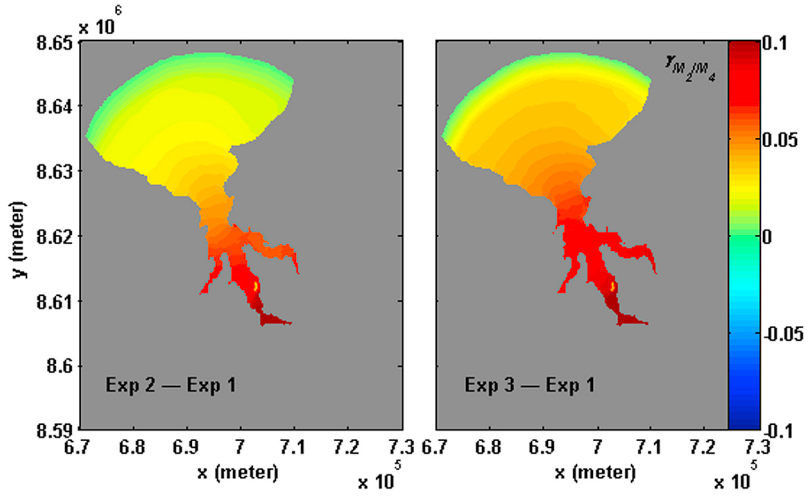

Figure 12. Changes in the tidal asymmetry skewness γ_{M_2/M_4} of the water areas. (left) Mangrove areas removed (Experiment 2 minus Experiment 1) and (right) mangrove areas and tidal flats removed (Experiment 3 minus Experiment 1).

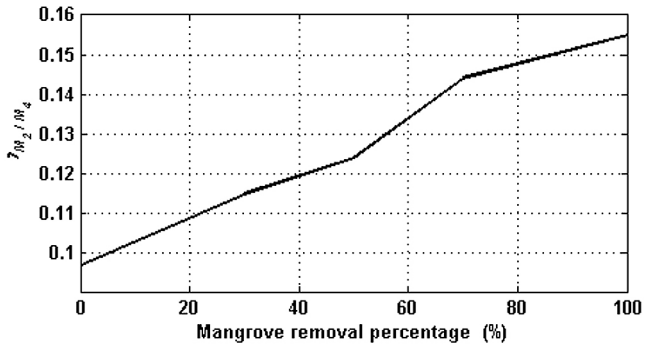

Figure 13. Tidal asymmetry γ_{M_2/M_4} as a function of percentage mangrove area removal in the East Arm near Station Blay.

respectively, compared with those of the reference model; the time at which the maximum M_4 current occurs is almost 0.5 h earlier.

[36] In Experiment 3, small changes occur in the M_2 amplitude and phase compared with those of the reference model, whereas the M_4 amplitude/phase increases/advances by 75%/28°, respectively. The M_2/M_4 currents experience reductions of 45.7%/40.0%, respectively, compared with those of the reference model; the time at which the maximum M_4 current occurs is about 1 h earlier.

[37] According to equation (5), the variations in the M_2 and M_4 amplitudes and phases lead to changed tidal asymmetry, measured by γ_{M_2/M_4}. The tidal asymmetry in Darwin Harbour is discussed in the next section.

4.3. Effects of Mangrove Areas and Tidal Flats on Tidal Asymmetry

[38] If the mangrove areas are completely removed, the tidal asymmetry skewness γ_{M_2/M_4} increases in all water areas, with the maximum increase being about 0.1(100%) in the arms (Figure 12, left). If the tidal flats are also completely removed (Experiment 3), γ_{M_2/M_4} experiences an increase of 0.15 in the arms (Figure 12, right). The same trend occurs for γ_1, calculated using equation (4).

[39] The increased tidal asymmetry skewness in Experiments 2 and 3 indicate that removal of the mangrove areas or tidal flats can amplify tidal asymmetry, which can lead to greater flood dominance in the harbor.

[40] The mangrove areas are removed incrementally from Experiment 4 to Experiment 6 to further examine their impact on tidal asymmetry in the harbor. Compared with Experiment 1, the asymmetry skewness γ_{M_2/M_4} in all water areas increases when first the mangrove areas around the East Arm are removed (Experiment 4: about 30% of the total mangrove area removed). The skewness γ_{M_2/M_4} increases progressively with the further removal of the mangrove areas on the east side of the Middle Arm (Experiment 5: 50% of the total mangrove area removed) and then all around the Middle Arm (Experiment 6: 70% of the total mangrove area removed). The maximum increase in tidal asymmetry occurs if 100% of the mangrove areas are removed, as already shown in Experiment 2.

[41] The variations in tidal asymmetry skewness γ_{M_2/M_4} in the East Arm near Station Blay as a function of percentage mangrove removal are shown in Figure 13. The relationship between percentage removal and the asymmetry is approximately linear. The tidal asymmetry skewness increases by 0.1, about 100%, compared with that of the reference model, if all the mangrove areas are removed. Therefore, the mangrove areas and tidal flats serve as important buffer zones for dampening tidal asymmetry, which affects the sediment transport patterns in the estuaries.

5. Conclusions

[42] An unstructured grid coastal ocean model (FVCOM) was employed to simulate the hydrodynamics in Darwin Harbour: the actual tides were well reproduced by this model. The model values for the M_2 and S_2 amplitudes, phases and maximum tidal current speeds at Station Blay are in good agreement with the observed values in both magnitude and trend from the bottom to the surface. The model therefore provides a reasonable simulation of the tidal dynamics in the harbor.

[43] The results indicate that the hydrodynamics of Darwin Harbour are complex and driven mainly by tides, with the effects of wind and rivers being small. The harbor is semidiurnal: the M_2 tide is predominant, with an amplitude of about 1.7 m, followed by the S_2 tide. Current flow is dominated by tides; the preliminary modeling analysis demonstrated that the current speed reaches a maximum of more than 3.0 m s^{-1} at the surface of the Middle Arm. The current speed decreases gradually from the surface to the bottom. The Middle Arm (shallower than 10.0 m) and the channel (about 25.0 m deep) have the largest (33.5%) and smallest (24.8%) decreases, respectively.

[44] A series of numerical experiments was carried out to help understand the overall physical processes in the harbor, especially the effects of mangrove areas and tidal flats on the tides. These experiments, sensitivity tests, indicated that the mangrove areas and tidal flats play key roles in modulating the tides and in the water flow dynamics of the estuary, tidal flats and mangrove areas. In Darwin Harbour, removal of mangrove areas and tidal flats would dampen the M_2 amplitude due to the decreased shoaling effects in the inner harbor, but would generate a greater M_4 amplitude. With mangrove areas and tidal flats removed, the amplitude of M_2 would increase/decrease slightly (<1.0%) in the outer harbor/inner harbor and the arms, respectively, and the M_2 phase advance by a maximum of 4° over all the water areas. The M_4 amplitude would increase by 75.0% in the arms and the phase increase/decrease by up to 30°/40° in the outer harbor/inner harbor and the arms, respectively.

[45] Mangrove areas and tidal flats affect tidal asymmetry due to their control of the amplitudes and phases of the tides. This study showed that these areas significantly reduce tidal asymmetry: for example, the tidal elevation skewness would increase by 100% and 120% in the Middle Arm, if the mangrove areas and mangroves plus tidal flats, respectively, were removed. The skewness varies linearly with the percentage of mangrove removal near Station Blay in the East Arm. As tidal asymmetry strongly affects sediment transport in the estuaries, care must be taken with any reclamation of the mangrove areas and tidal flats around the harbor watershed. An overall understanding of the hydrodynamics of Darwin Harbour will benefit the future study of its sedimentary dynamics.

[46] This study is site-specific, but our findings have a wider applicability to the effects of mangrove areas and tidal flats on tides and sediment transport in harbors and estuaries.

[47] **Acknowledgments.** L. Li acknowledges the support of the China Scholarship Council. X. H. Wang and D. Williams were supported by a 2011 Australian Research Council/ Linkage Project—LP110100652. This work was also supported by the National Computational Infrastructure National Facility at the Australian National University. We thank two anonymous referees for many helpful suggestions and Peter McIntyre for editorial support. This is a publication of the Sino-Australian Research Centre for Coastal Management, paper 8.

References

Blumberg, A. F., and G. L. Mellor (1987), A description of a three-dimensional coastal ocean circulation model, in *Three-Dimensional Coastal Ocean Models*, *Coastal Estuarine Sci.*, vol. 4, edited by N. S. Heaps, pp. 1–16, AGU, Washington, D. C., doi:10.1029/CO004p0001.

Chen, C., H. Liu, and R. C. Beardsley (2003), An unstructured grid, finite-volume, three-dimensional, primitive equations ocean model: Application to coastal ocean and estuaries, *J. Atmos. Oceanic Technol.*, *20*, 159–186, doi:10.1175/1520-0426(2003)020<0159:AUGFVT>2.0.CO;2.

Chen, C., R. C. Beardsley, and G. Cowles (2006), An unstructured grid, finite volume coastal ocean model: FVCOM user manual, 2nd ed., *Rep. SMAST/UMASSD-06-0602*, Mar. Ecosyst. Dyn. Model. Lab., Univ. of Mass., Dartmouth.

Egbert, G. D., S. Y. Erofeeva, and R. D. Ray (2010), Assimilation of altimetry data for nonlinear shallow-water tides: Quarter-diurnal tides of the northwest European shelf, *Cont. Shelf Res.*, *30*(6), 668–679, doi:10.1016/j.csr.2009.10.011.

Emery, W. J., and R. E. Thomson (2001), *Data Analysis Methods in Physical Oceanography*, 2nd ed., Elsevier, Amsterdam.

Godin, G. (1991), The analysis of tides and currents, in *Tidal Hydrodynamics*, edited by B. B. Parker, pp. 675–708, John Wiley, New York.

Hamrick, J. M. (1992), *A Three-Dimensional Environmental Fluid Dynamics Computer Code: Theoretical and Computational Aspects*, *Spec. Rep. Appl. Mar. Sci. Ocean Eng.*, vol. 317, Va. Inst. of Mar. Sci., Coll. of William and Mary, Gloucester Point, Va.

Li, L., X. H. Wang, H. Sidhu, and D. Williams (2011), Modelling of three dimensional tidal dynamics in Darwin Harbour, Australia, *ANZIAM J.*, *52*, C103–C123.

Mazda, Y., M. Magi, M. Kogo, and P. N. Hong (1997), Mangroves as a coastal protection from waves in the Tong King delta, Vietnam, *Mangroves Salt Marshes*, *1*(2), 127–135, doi:10.1023/a:1009928003700.

Mehta, A. J. (1988), Laboratory studies on cohesive sediment deposition and erosion, in *Physical Processes in Estuaries*, edited by J. Dronkers and W. van Leussen, pp. 427–445, Springer, Berlin.

Mellor, G. L., and T. Yamada (1982), Development of a turbulence closure model for geophysical fluid problems, *Rev. Geophys.*, *20*(4), 851–875, doi:10.1029/RG020i004p00851.

Nidzieko, N. J. (2010), Tidal asymmetry in estuaries with mixed semidiurnal/diurnal tides, *J. Geophys. Res.*, *115*, C08006, doi:10.1029/2009JC005864.

Smagorinsky, J. (1963), General circulation experiments with the primitive equations I. The basic experiment, *Mon. Weather Rev.*, *91*, 99–164, doi:10.1175/1520-0493(1963)091<0099:GCEWTP>2.3.CO;2.

Song, D., X. H. Wang, A. E. Kiss, and X. Bao (2011), The contribution to tidal asymmetry by different combinations of tidal constituents, *J. Geophys. Res.*, *116*, C12007, doi:10.1029/2011JC007270.

Walton, T. L., Jr. (2002), Tidal velocity asymmetry at inlets, *Rep. ERDC/CHL CHETN-IV-47*, U.S. Army Eng. Res. and Dev. Cent., Vicksburg, Miss. [Available at http://chl.erdc.usace.army.mil/library/publications/chetn/pdf/chetn-iv-47.pdf.]

Water Monitoring Branch (2005), The health of the aquatic environment in the Darwin Harbour region, 2004, *Rep. 5/2005D*, Nat. Resour. Manage. Div., Dep. of Nat. Resour., Environ., and the Arts, Darwin, North. Territ., Australia. [Available at http://www.nretas.nt.gov.au/natural-resource-management/water/aquatic/ausrivas/darwinharbour.]

Williams, D. (2009), Part 1: Hydrodynamics and sediment transport, in *Dredging of Sand From Darwin Harbour, Hydrographic and Marine Life*, report, pp. 1–33, Aust. Inst. of Mar. Sci., Arafura Timor Res. Facil., Brinkin, North. Territ., Australia.

Williams, D., E. Wolanski, and S. Spagnol (2006), Hydrodynamics of Darwin Harbour, in *The Environment in Asia Pacific Harbours*, edited by E. Wolanski, pp. 461–476, Springer, Dordrecht, Netherlands, doi:10.1007/1-4020-3655-8_26.

Wright, L. D., J. D. Boon, J. P. Xu, and S. C. Kim (1992), The bottom boundary layer of the bay stem plains environment of lower Chesapeake Bay, *Estuarine Coastal Shelf Sci.*, *35*(1), 17–36, doi:10.1016/S0272-7714(05)80054-X.